Density-functional theory of pair correlations in metallic hydrogen

Hong Xu[1] and Jean-Pierre Hansen[2]

[1]*Département de Physique des Matériaux (UMR 5586 du CNRS), Université Claude Bernard-Lyon 1,
43 Boulevard du 11 Novembre 1918, 69622 Villeurbanne Cedex, France*
[2]*Laboratoire de Physique (URA 1325 du CNRS), Ecole Normale Supérieure de Lyon, 46 Allée d'Italie, 69346 Lyon Cedex 07, France*

The pair correlations in the metallic phase of hydrogen are reconsidered on the basis of a simple density-functional formulation of the free energy of the ion-electron plasma, which includes a square-gradient correction to the Thomas-Fermi kinetic energy of the degenerate electrons. A robust prescription is given for the prefactor of the square-gradient correction. The functional leads to a hypernetted-chain–like closure for the ion-ion and ion-electron correlation functions, which is solved iteratively, in conjunction with the coupled Ornstein-Zernike equations relating the matrices of pair and direct correlation functions. The resulting structure agrees well with available *ab initio* simulation data based on the Kohn-Sham functional. A density- and temperature-dependent effective ion-ion pair potential is obtained by formally reducing the initial two-component system to a one-component fluid of pseudoatoms. The results show strong deviations of the present nonlinear theory from the standard linear screening approach for $r_s > 1$ (where r_s is the usual inverse density parameter equal to the ratio of the electron sphere radius over the Bohr radius). The long-wavelength ion density fluctuations are strongly enhanced as the density drops, and at the lowest density ($r_s = 1.5$) the ion-ion pair structure and effective potential exhibit an unusual behavior, at the lower temperature explored in this paper ($T = 3 \times 10^3$ K), which may be interpreted as a precursor to an incipient plasma-insulator transition. Thermodynamic properties are estimated from the pair structure. The influence of nonlinear electron polarization on the equation of state is found to be surprisingly small, but the isothermal compressibility increases sharply at the lowest density. [S1063-651X(98)03501-6]

PACS number(s): 05.30.Fk, 61.20.−p, 31.15.Ew

I. INTRODUCTION

Metallic systems, including metals under normal conditions and pressure-ionized (metallic) hydrogen, are basically two-component plasmas made up of an ionic species and "free" conduction electrons. The ionic species may be either fully stripped, i.e., reduced to bare nuclei, or retain tightly bound core electrons; except under high-density conditions (as may occur in degenerate stellar matter), the de Broglie thermal wavelength associated with the ions is much less than the mean interionic spacing, so the ionic component may be safely described by classical statistical mechanics. On the other hand, the density of metallic systems is usually sufficiently high for the Fermi temperature T_F associated with the free electrons to greatly exceed the thermodynamic temperature T. In other words, the degeneracy parameter $\theta = T/T_F \ll 1$, so, to a good approximation, the electronic component may be regarded as fully degenerate: For any "frozen" ionic configuration, the inhomogeneous gas of conduction electrons is in its ground state. The fact that metallic systems may, over a broad range of physical conditions, be assimilated to a neutral mixture of two charged fluids, one classical and the other degenerate, must of course be traced back to the large mass ratio of ions and electrons. This large mass ratio also justifies the adiabatic or Born-Oppenheimer approximation, whereby the electronic component may be regarded as readjusting its ground state quasi-instantaneously to the much slower ionic motions. On the time scale of the latter, the electrons may be regarded as forming an inhomogeneous, degenerate, interacting Fermi fluid in the "external" field provided by the ions in their

instanteneous configuration. This inhomogeneous electron fluid is most efficiently described within the density-functional theory (DFT) developed by Hohenberg, Kohn, and Sham [1,2] and generalized to finite temperatures by Mermin [3]. A conceptually similar formulation has been proposed by Percus [4] for classical inhomogeneous fluids.

For a number of applications, it is convenient to consider both components, i.e., the classical ionic fluid and the degenerate electronic fluid, to be inhomogeneous on average. In other words, the equilibrium state of a metallic system may be characterized by two spatially varying (local) densities $\rho_1(\mathbf{r})$ and $\rho_2(\mathbf{r})$ associated with the ions (species 1) and the electrons (species 2). This point of view has been be adopted in a DFT description of freezing of an ion-electron system [5] or to derive a set of equations for a quantitative description of pair correlations in a dense ion-electron plasma. A number of papers deal with this second application. They differ by the treatment of the kinetic-energy part in the energy functional of the degenerate electrons. In the work of Dharma-wardana and Perrot [6] and Chihara [7], the Kohn-Sham independent-particle orbital point of view [2] is adopted, while in the more recent work of Ofer *et al.* [8], the simpler Thomas-Fermi approximation to the kinetic energy is used. The two types of electron energy functionals are combined with a hypernetted-chain (HNC) closure relation [9] for ion-ion correlations. It is interesting to note that these two points of view also show up in the *ab-initio* simulations of ion-electron systems: In the method of Car and Parrinello [10], the Kohn-Sham representation is used, while the Thomas-Fermi kinetic-energy functional [11] or improvements thereof [12] have been successfully used in "orbital-

free'' first-principles simulations. The latter seem to be particularly well adapted to metallic systems, for a number of technical reasons [13]. Both Kohn-Sham [14,15] and orbital-free [11] simulations have been applied to metallic hydrogen, which is the object of the present paper.

We adopt the orbital-free point of view for the electronic kinetic-energy functional, going beyond the Thomas-Fermi approximation [8] (which is expected to be particularly poor for hydrogen), by including a square-gradient correction [16], which is crucial for a proper description of the electron density very close to the nuclei. The approach may be further improved by going to a hybrid functional proposed by Perrot [17], which incorporates the correct linear response of the eletron fluid. The DFT formulation is restricted to fully ionized plasmas in this paper, i.e., the ions reduce to bare nuclei; the presence of bound states (core electrons) may be accounted for by the use of ion-electron pseudopotentials or by a self-consistent DFT scheme as proposed by Chihara [18] within the Kohn-Sham formulation. As in Ref. [6–8], the HNC closure is used to determine ion-ion correlations.

The present DFT of ion-ion and ion-electron correlations, expounded in Secs. II–IV, is applied to hydrogen (i.e., a mixture of protons and electrons) in Secs. V and VI, over the range of densities $r_s \leq 1.5$, where hydrogen is expected to be metallic (no bound states). In Sec. VII we consider the problem of calculating thermodynamic properties of metallic hydrogen, a question that has received very little attention in previous DFT and simulation work. Concluding remarks are contained in Sec. VIII.

II. IONS AND ELECTRONS

Within the ''two-fluid'' picture, a metallic system is made up of a classical ionic component (species 1), containing n_1 ions (nuclei) of charge $Z_1 e$ and mass m_1 per unit volume, and a degenerate electronic component (species 2), containing n_2 electrons of charge $-e$ and mass m_2 per unit volume. Charge neutrality implies $Z n_1 = n_2$. It is convenient to adopt atomic units, where $e = 1$, $m_2 = 1$, and $\hbar = 1$; lengths are then in units of the Bohr radius ($a_B = \hbar^2/m_2 e^2 = 1$) and energies are expressed in hartrees ($e^2/a_B = 1$), i.e. multiples of 27.2 eV. The radius of a sphere containing, on average, one electron is $r_s = (3/4\pi n_2)^{1/3}$, while the corresponding ion-sphere radius is $a_1 = r_s Z^{1/3}$. The Fermi wave number $k_F = (9\pi/4)^{1/3}/r_s$, while the Thomas-Fermi (TF) wave number is $k_{TF} = (12/\pi)^{1/3} r_s^{1/2}$.

The Hamiltonian may be decomposed into ionic and electronic parts and an ion-electron coupling term

$$H = H_1 + H_2 + V_{12} \tag{1}$$

and

$$H_\alpha = K_\alpha + V_{\alpha\alpha}, \tag{2}$$

where K_α and $V_{\alpha\alpha}$ denote the kinetic and the potential energy of interaction of species α. Introducing the microscopic density operators

$$\widetilde{\rho}_\alpha(\mathbf{r}) = \sum_{i=1}^{N_\alpha} \delta(\mathbf{r} - \mathbf{r}_{i,\alpha}), \tag{3}$$

where $\mathbf{r}_{i,\alpha}$ is the position of the ith particle of species α, and noting that $Z_1 \equiv Z$ and $Z_2 \equiv -1$, the potential-energy term $V_{\alpha\beta}$ may be cast in the compact form

$$V_{\alpha\beta} = \frac{Z_\alpha Z_\beta}{1 + \delta_{\alpha\beta}} \int d\mathbf{r} \int d\mathbf{r}' [\widetilde{\rho}_\alpha(\mathbf{r}) \widetilde{\rho}_\beta(\mathbf{r}')$$
$$- \delta_{\alpha\beta} \widetilde{\rho}_\alpha(\mathbf{r}) \delta(\mathbf{r} - \mathbf{r}')] \frac{1}{|\mathbf{r} - \mathbf{r}'|}. \tag{4}$$

Full ionization has been assumed in writing Eq. (4), i.e., the interactions between all particles are purely Coulombic. Integrations are over the total volume V of the system.

To discard any divergence problems of the separate contributions H_1, H_2, and V_{12} in the thermodynamic limit, it is convenient to add and substract a uniform (neutralizing) background, of (charge) density $n_0 \equiv n_2$ [19]. The Hamiltonian (1) is then recast in the form

$$H = H_1' + H_2' + V_{12}', \tag{5}$$

where

$$H_1' = H_1 + V_{00} + V_{01}, \tag{6a}$$

$$H_2' = H_2 - V_{00}, \tag{6b}$$

$$V_{12}' = V_{12} - V_{01}, \tag{6c}$$

with

$$V_{00} = \frac{n_0^2}{2} \int d\mathbf{r} \int d\mathbf{r}' \frac{1}{|\mathbf{r} - \mathbf{r}'|}, \tag{7a}$$

$$V_{01} = -n_0 Z_1 \int d\mathbf{r} \int d\mathbf{r}' \frac{\widetilde{\rho}_1(\mathbf{r})}{|\mathbf{r} - \mathbf{r}'|}. \tag{7b}$$

Note that H_1' is precisely the Hamiltonian of the widely studied (classical) one-component plasma (OCP) [20], while H_2' is that of jellium, introduced by Wigner [21] as a model for electrons in metals. In the ultrahigh-density limit $r_s \to 0$, the ratio of the TF wavelength $\lambda_{TF} = 1/k_{TF} \approx r_s^{1/2}$ over the mean distance between electrons, approximately equal to r_s, diverges, so the electronic component behaves like a rigid (nonpolarizable) background; the ion-electron coupling (6c) becomes negligible, so that the two fluids decouple; and the hydrogen plasma behaves like the superposition of a classical OCP and a fully degenerate jellium. As r_s increases, electron polarization effects become increasingly important. A linear screening treatment of the ion-electron coupling is expected to be accurate up to $r_s \approx 0.5$ [22,14]. At lower densities, nonlinear screening becomes important, which requires the use of a nonlinear DFT, like that proposed in this paper. In compressed hydrogen a metal-insulator transition to the molecular phase is expected beyond $r_s = 1.5$ (see, e.g., Ref. [15]), which means that bound states become important. Their quantitative treatment is beyond the scope of the simple DFT used in the present work, so that explicit calculations will be restricted to the range $0.5 \leq r_s \leq 1.5$, which corresponds to a decrease by a factor 27 in density. The degeneracy parameter $\theta = 2(4/9\pi)^{2/3} r_s^2 (k_B T)$ a.u. ≈ 1.72

$10^{-6} r_s^2 T$ K for hydrogen. The range of the calculations will be limited to temperatures, such that $\theta \leq 0.08$, so that the electron fluid can always be assumed, to an excellent approximation, to be in its ground state. A convenient dimensionless Coulomb coupling parameter is that routinely used for the OCP, namely, $\Gamma = e^2/a_B r_s k_B T = 1/r_s(k_B T)$ a.u.

III. THE FREE-ENERGY FUNCTIONAL

If the ion-electron plasma is subjected to external potentials $\phi_\alpha(\mathbf{r})$ that couple to the microscopic densities (3), extra terms must be added to the Hamiltonian H; denoting the unperturbed Hamiltonian defined in Eqs. (1) or (5) by H_0, the total Hamiltonian now reads

$$H = H_0 + \sum_{\alpha=1,2} \int \phi_\alpha(\mathbf{r}) \widetilde{\rho}_\alpha(\mathbf{r}) d\mathbf{r}. \qquad (8)$$

The external potentials will induce spatial inhomogeneity in the plasma, characterized by the one-particle densities or density profiles:

$$\rho_\alpha(\mathbf{r}) = \langle \widetilde{\rho}_\alpha(\mathbf{r}) \rangle, \quad \alpha = 1,2. \qquad (9)$$

The grand partition function is

$$\Xi(\beta, \mu_1, \mu_2) = \sum_{N_1} \sum_{N_2} \mathrm{Tr}[\exp\{-\beta(H - \mu_1 N_1 - \mu_2 N_2)\}], \qquad (10)$$

where $\beta = 1/k_B T$. The trace is over the phase space of the ions and over the quantum states of the electrons, and the sums over N_1 and N_2 are restricted by the charge neutrality constraint $N_2 = Z N_1$; μ_α is the chemical potential of species α. The ground potential divided by $-k_B T$, $\Omega = \ln \Xi$, is a functional of

$$\Psi_\alpha(\mathbf{r}) = \beta[\mu_\alpha - \phi_\alpha(\mathbf{r})], \quad \alpha = 1,2. \qquad (11)$$

The first and second functional derivatives of Ω yield the one-particle densities and the matrix of nonlocal linear-response functions or susceptibilities:

$$\frac{\delta \Omega[\Psi_1, \Psi_2]}{\delta \Psi_\alpha(\mathbf{r})} = \rho_\alpha(\mathbf{r}), \qquad (12a)$$

$$\frac{\delta^2 \Omega[\Psi_1, \Psi_2]}{\delta \Psi_\alpha(\mathbf{r}) \delta \Psi_\beta(\mathbf{r}')} = \frac{\delta \rho_\alpha(\mathbf{r})}{\delta \Psi_\beta(\mathbf{r}')} = \chi_{\alpha\beta}(\mathbf{r}, \mathbf{r}'). \qquad (12b)$$

According to linear response theory [23],

$$\chi_{\alpha\beta}(\mathbf{r}, \mathbf{r}') = \int_0^{\beta\hbar} \frac{d\lambda}{\beta\hbar} \langle \Delta \widetilde{\rho}_\alpha(\mathbf{r}; -i\lambda) \Delta \widetilde{\rho}_\beta(\mathbf{r}') \rangle, \qquad (13)$$

where $\Delta \widetilde{\rho}_\alpha(\mathbf{r}; -i\lambda)$ is the deviation of the local-density operator from its mean at the imaginary time $-i\lambda$ (Heisenberg representation). In the classical ($\hbar \to 0$) limit, applicable to ion-ion and ion-electron correlations

$$\chi_{\alpha\beta}^{cl}(\mathbf{r}, \mathbf{r}') = \langle \widetilde{\rho}_\alpha(\mathbf{r}) \widetilde{\rho}_\beta(\mathbf{r}') \rangle - \langle \widetilde{\rho}_\alpha(\mathbf{r}) \rangle \langle \widetilde{\rho}_\beta(\mathbf{r}') \rangle$$

$$= \rho_\alpha(\mathbf{r}) \rho_\beta(\mathbf{r}') h_{\alpha\beta}(\mathbf{r}, \mathbf{r}'), \qquad (14)$$

where $h_{\alpha\beta}(\mathbf{r}, \mathbf{r}') = g_{\alpha\beta}(\mathbf{r}, \mathbf{r}') - 1$ is the two-point (or pair) correlation function, while $g_{\alpha\beta}$ denotes the pair distribution function (PDF) for particles of species α and β.

A standard Legendre transformation takes us from the grand potential to the dimensionless intrinsic Helmholtz free energy, a functional of the density profiles

$$F[\rho_1, \rho_2] = -\Omega[\Psi_1, \Psi_2] + \sum_\alpha \int \rho_\alpha(\mathbf{r}) \Psi_\alpha(\mathbf{r}) d\mathbf{r}. \qquad (15)$$

F admits the functional derivatives

$$\frac{\delta F[\rho_1, \rho_2]}{\delta \rho_\alpha(\mathbf{r})} = \Psi_\alpha(\mathbf{r}), \quad \alpha = 1,2 \qquad (16a)$$

$$\frac{\delta^2 F[\rho_1, \rho_2]}{\delta \rho_\alpha(\mathbf{r}) \delta \rho_\beta(\mathbf{r}')} = \frac{\delta \Psi_\alpha(\mathbf{r})}{\delta \rho_\beta(\mathbf{r}')} = \chi_{\alpha\beta}^{-1}(\mathbf{r}, \mathbf{r}'), \qquad (16b)$$

where the matrix χ^{-1} is the functional inverse of the susceptibility matrix in Eq. (12b).

The free-energy functional is separated into ideal and excess (nonideal) parts in the usual way:

$$F[\rho_1, \rho_2] = F_1^{(0)}[\rho_1] + F_2^{(0)}[\rho_2] + F^{ex}[\rho_1, \rho_2]. \qquad (17)$$

The inverse susceptibility matrix splits accordingly into two parts

$$\chi_{\alpha\beta}^{-1} = \chi_{\alpha\beta}^{(0)-1}(\mathbf{r}, \mathbf{r}') - c_{\alpha\beta}(\mathbf{r}, \mathbf{r}'), \qquad (18)$$

where the first (ideal) term is diagonal

$$\chi_{\alpha\beta}^{(0)-1}(\mathbf{r}, \mathbf{r}') = \chi_\alpha^{(0)-1}(\mathbf{r}, \mathbf{r}') \delta_{\alpha\beta}, \qquad (19)$$

while the second (nonideal) term is the matrix of direct correlation functions (DCF's). For the classical ions ($\alpha = 1$)

$$\chi_1^{(0)-1}(\mathbf{r}, \mathbf{r}') = \frac{1}{\rho_1(\mathbf{r})} \delta(\mathbf{r} - \mathbf{r}'). \qquad (20)$$

Expressing the fact that the matrices χ and χ^{-1} are functional inverses of each other and using Eq. (14) for χ_{11} and χ_{12}, together with Eq. (20), one easily arrives at the coupled Ornstein-Zernike (OZ) relations (see, e.g., Ref. [18])

$$h_{11}(\mathbf{r}, \mathbf{r}') = c_{11}(\mathbf{r}, \mathbf{r}') + h_{11}*(\rho_1 c_{11})(\mathbf{r}, \mathbf{r}')$$
$$+ h_{12}*(\rho_2 c_{12})(\mathbf{r}, \mathbf{r}'), \qquad (21a)$$

$$h_{12}*(\rho_2 \chi_2^{(0)-1})(\mathbf{r}, \mathbf{r}') = c_{12}(\mathbf{r}, \mathbf{r}') + h_{11}*(\rho_1 c_{12})(\mathbf{r}, \mathbf{r}')$$
$$+ h_{12}*(\rho_2 c_{22})(\mathbf{r}, \mathbf{r}'), \qquad (21b)$$

$$(\chi_{22} - \chi_2^{(0)})*(\chi_2^{(0)-1})(\mathbf{r}, \mathbf{r}') = (\rho_1 h_{12})*(\rho_2 c_{12})(\mathbf{r}, \mathbf{r}')$$
$$+ \chi_{22}*(c_{22})(\mathbf{r}, \mathbf{r}'), \qquad (21c)$$

where the asterisk denotes a convolution product. These OZ relations will be used later in their form appropriate for a homogeneous fluid, for which translational invariance implies that $\rho_\alpha(\mathbf{r}) = n_\alpha$ and $f_{\alpha\beta}(\mathbf{r}, \mathbf{r}') = f_{\alpha\beta}(\mathbf{r} - \mathbf{r}')$ for any two-point function. Fourier transformation (FT) reduces the above OZ relations to the form

$$\hat{h}_{11}(k) = \hat{c}_{11}(k) + n_1\hat{h}_{11}(k)\hat{c}_{11}(k) + n_2\hat{h}_{12}(k)\hat{c}_{12}(k),$$
$$(22a)$$

$$\frac{n_2\hat{h}_{12}(k)}{\hat{\chi}_2^{(0)}(k)} = \hat{c}_{12}(k) + n_1\hat{h}_{11}(k)\hat{c}_{12}(k) + n_2\hat{h}_{12}(k)\hat{c}_{22}(k),$$
$$(22b)$$

$$\frac{\hat{\chi}_{22}(k) - \hat{\chi}_2^{(0)}(k)}{\hat{\chi}_2^{(0)}(k)} = \hat{c}_{22}(k)\hat{\chi}_{22}(k) + n_1n_2\hat{h}_{12}(k)\hat{c}_{12}(k).$$
$$(22c)$$

The susceptibility of noninteracting electrons is the well-known Lindhard function [24]

$$\hat{\chi}_2^{(0)}(k) = -\frac{k_F^2}{\pi^2}\left[\frac{1}{2} + \frac{1-q^2}{4q}\ln\left|\frac{1+q}{1-q}\right|\right], \qquad (23)$$

where $q = k/2k_F$.

By integrating the excess part of Eq. (16b) along a linear path in one-particle density space, starting from a uniform reference state, with the same macroscopic density n_α,

$$\rho_\alpha(\mathbf{r};\xi) = n_\alpha + \xi[\rho_\alpha(\mathbf{r}) - n_\alpha] = n_\alpha + \xi\Delta\rho_\alpha(\mathbf{r}), \quad 0 \leq \xi \leq 1,$$
$$(24)$$

one arrives at the following, exact expression for the intrinsic excess free energy of the ion-electron system:

$$\Delta F^{ex} = F^{ex}[\rho_1,\rho_2] - F_0^{ex}(n_1,n_2)$$
$$= -\sum_\alpha \sum_\beta \int_0^1 d\xi(1-\xi)\int d\mathbf{r}\int d\mathbf{r}'\Delta\rho_\alpha(\mathbf{r})$$
$$\times c_{\alpha\beta}[\rho_1(\xi),\rho_2(\xi);\mathbf{r},\mathbf{r}']\Delta\rho_\beta(\mathbf{r}'). \qquad (25)$$

The direct correlation function associated with the intermediate one-particle densities (24) may be expanded in powers of ξ around those associated with the uniform densities n_α. In the HNC approximation [9], only the lowest-order term is retained, i.e.

$$c_{\alpha\beta}[\rho_1(\xi),\rho_2(\xi);\mathbf{r},\mathbf{r}'] \approx c_{\alpha\beta}^0(n_1,n_2;\mathbf{r}-\mathbf{r}'). \qquad (26)$$

The corresponding, approximate, expression for the excess free energy reads

$$\Delta F^{ex} = -\frac{1}{2}\sum_\alpha \sum_\beta \int d\mathbf{r}\int d\mathbf{r}'\Delta\rho_\alpha(\mathbf{r})$$
$$\times c_{\alpha\beta}^0(n_1,n_2;\mathbf{r}-\mathbf{r}')\Delta\rho_\beta(\mathbf{r}')$$
$$\equiv \Delta F_{11}^{ex} + \Delta F_{12}^{ex} + \Delta F_{22}^{ex}. \qquad (27)$$

For a purely *classical* mixture, the free-energy functional (27) yields, via Eq. (16a) and the Percus identification of the external potential as that due to a fixed particle of species α [4], to the well-known HNC closure relation [9]. These, together with the OZ relations (21) adapted to the classical limit, form a closed set to compute the three PDF's $g_{\alpha\beta}(r)$. In the ion-electron case, where the electrons are degenerate, the nontrivial relation (13) between χ_{22} and the electron den-

sity correlation function requires an additional approximation to be made to arrive at a closed set of equations [6,7].

The approximation made in the present work is most easily understood by rewriting the dimensionless intrinsic free energy in the form

$$F[\rho_1,\rho_2] = F_1^{(0)}[\rho_1] + F_2^{(0)}[\rho_2] + F_0^{ex}(n_1,n_2) + \Delta F_{11}^{ex}[\rho_1]$$
$$+ \Delta F_{12}^{ex}[\rho_1,\rho_2] + \Delta F_{22}^{ex}[\rho_2]. \qquad (28)$$

In Eq. (27), $F_1^{(0)}[\rho_1]$ for the classical ions is known exactly:

$$F_1^{(0)}[\rho_1] = \int \rho_1(\mathbf{r})\{\ln[\rho_1(\mathbf{r})\Lambda_1^3] - 1\}d\mathbf{r}. \qquad (29)$$

The contributions ΔF_{11}^{ex} and ΔF_{12}^{ex} are given by the HNC-like approximation (27). The remaining terms, which are functionals of ρ_2, are proportional to the intrinsic ground-state energy of the inhomogeneous electron gas, as long as $\theta \ll 1$:

$$k_B T \Delta F_2[\rho_2] = k_B T\{\Delta F_2^{(0)}[\rho_2] + \Delta F_{22}^{ex}[\rho_2]\}$$
$$= E[\rho_2] - E(n_2). \qquad (30)$$

The terms corresponding to the homogeneous ion-electron plasma are funtions of the macroscopic densities n_1 and n_2, not functionals of ρ_1 and ρ_2, and are hence irrelevent for what follows.

In Refs. [6] and [7], $E[\rho_2]$ is calculated within the Kohn-Sham approximation. In this work a simpler, orbital-free representation is used. The functional is split into its kinetic (noninteracting), Hartree, and exchange contributions, according to

$$E[\rho_2] = E_K[\rho_2] + E_H[\rho_2] + E_X[\rho_2]. \qquad (31)$$

For the kinetic-energy functional, we adopt either of two approximations.

(a) One is Thomas-Fermi plus square-gradient correction (von Weizsácker) approximation [TF-W(λ)]

$$E_K[\rho_2] = C_K\int [\rho_2(\mathbf{r})]^{5/3}d\mathbf{r} + \frac{\lambda}{8}\int \frac{|\nabla\rho_2(\mathbf{r})|^2}{\rho_2(\mathbf{r})}d\mathbf{r},$$
$$(32a)$$

with $C_K = 3(3\pi^2)^{2/3}/10$. The precise value of λ has been the object of a long-standing debate in atomic physics [16]. A rigorous gradient expansion predicts $\lambda = 1/9$, while in von Weizsäcker's original derivation $\lambda = 1$. This value leads to the exact linear response of the noninteracting electron gas on the short-distance (large-wave-number) scale, whereas $\lambda = 1/9$ guarantees the correct linear response at large distances (i.e., small wave numbers). Empirically it is known that $\lambda \approx 1/5$ yields the best ground-state energies of many atoms [16].

(b) The other is functional proposed by Perrot, which interpolates correctly between these two regimes and guarantees the exact linear response [as described by the Lindhard susceptibility (23)] on all scales:

$$E_K[\rho_2] = C_K \int [\rho_2(\mathbf{r})]^{5/3} d\mathbf{r} + \frac{1}{8} \int \frac{|\boldsymbol{\nabla}\rho_2(\mathbf{r})|^2}{\rho_2(\mathbf{r})} d\mathbf{r}$$

$$+ \frac{V}{2} \sum_{\mathbf{k}} \left\{ \frac{1}{\chi_w(k)} - \frac{1}{\chi^{(0)}(k)} \right\} \hat{\rho}_2(\mathbf{k}) \hat{\rho}_2(-\mathbf{k}).$$

$$(32b)$$

In this equation λ has been chosen to be equal to 1. $\hat{\rho}_2(\mathbf{k})$ is the FT of the electron density profile $\rho_2(\mathbf{r})$, $\chi^{(0)}(k)$ is the Lindhard susceptibility (23) (the index 2 has been dropped), and $\chi_w(k)$ is the approximate susceptibility of the noninteracting electron gas, as derived from the kinetic-energy functional (32a) (with $\lambda = 1$), namely,

$$\chi_w(k) = -\frac{k_F}{\pi^2} \frac{1}{1 + 3q^2}, \qquad (33)$$

where again $q = k/2k_F$. It is easy to check that $\chi_w(k) \to \chi^{(0)}(k)$ when $q \to \infty$, as indicated earlier. The remaining terms in the energy functional (31) are taken to be

$$E_H[\rho_2] = \frac{1}{2} \int d\mathbf{r} \int d\mathbf{r}' \frac{\Delta\rho_2(\mathbf{r})\Delta\rho_2(\mathbf{r}')}{|\mathbf{r} - \mathbf{r}'|}, \qquad (34)$$

$$E_X[\rho_2] = C_X \int [\rho_2(\mathbf{r})]^{4/3} d\mathbf{r}, \qquad (35)$$

where the local-density approximation (LDA) has been adopted for the exchange term and $C_X = -3(3/\pi)^{1/3}/4$.

Within the same approximation, an electron correlation term could be easily added; in the range $r_s \lesssim 1.5$, which has been explored in this work, this term is expected to be very small and has been neglected for the sake of simplicity. Equations (28)–(35) completely define the free-energy functional of the ion-electron plasma used in the present work. Criteria for an optimum choice of the factor λ in the square-gradient correction, when the kinetic-energy functional (32a) is used, will be spelled out in the subsequent sections of the paper.

IV. A PRELIMINARY APPLICATION: THE ION-SPHERE MODEL

The functional defined in Sec. III will be applied first to a highly simplified model of the ion-electron plasma, namely, the so-called ion-sphere (IS) model. The IS model is itself a simplification of the Wigner-Seitz model for the description of ionic crystals, where the total volume is divided into N_1 identical, space-filling polyhedra, called Wigner-Seitz cells, having an ion in their center. In the ion-sphere model, the Wigner-Seitz polyhedron is replaced by a sphere of identical volume $v = V/N$ and hence of radius a_1. The ion, of charge Ze, is fixed at the center, while Z electrons are nonuniformly distributed over the volume v. Each sphere being electrically neutral, the total Coulomb interaction between different ion spheres vanishes, according to Gauss's theorem. It is hence sufficient to consider a single IS and to minimize the corresponding total-energy functional with respect to the spherically symmetric electron density profile $\rho_2(r)$, subject to the constraint
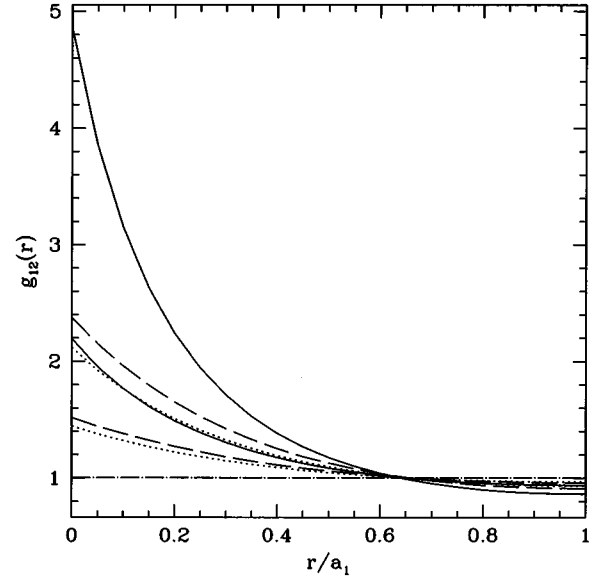

FIG. 1. $g_{12}(r)$ from the ion-sphere model with TFW(λ) and Perrot kinetic-energy functionals, at $r_s = 0.5$ and $r_s = 1$. The long-dashed lines represent $g_{12}(r)$'s from the Perrot functional, the solid lines those from the TFW functional with $\lambda = 0.41$, and the dotted lines those with $\lambda = 1$. For each functional used, the lower curve is for $r_s = 0.5$ and the upper curve for $r_s = 1$.

$$4\pi \int_0^{a_1} r^2 \rho_2(r) dr = Z. \qquad (36)$$

The "external" potential $\phi_2(r)$ is provided here by the central ion. When the kinetic-energy functional (32a) is adopted, the Euler-Lagrange equation associated with Eq. (16a), where $\Psi(r) = \mu_2 + Z/r$, reads

$$\frac{\lambda}{8} \left\{ \left[\frac{\rho_2'(r)}{\rho_2(r)} \right]^2 - \frac{2\rho_2''(r)}{\rho_2(r)} - \frac{4}{r} \frac{\rho_2'(r)}{\rho_2(r)} \right\} + \frac{5}{3} C_K[\rho_2(r)]^{2/3}$$

$$+ \frac{4}{3} C_X[\rho_2(r)]^{1/3} = \mu_2 - \Phi(r), \qquad (37)$$

where the total electrostatic potential $\Phi(r)$ is a solution of Poisson's equation

$$\Phi''(r) + \frac{2}{r} \Phi'(r) = 4\pi\rho_2(r), \quad r > 0, \qquad (38)$$

and satisfies the boundary conditions

$$\lim_{r \to 0} r\Phi(r) = Z, \qquad (39a)$$

$$\Phi'(r = a_1) = 0. \qquad (39b)$$

A similar albeit integro-differential Euler-Lagrange equation holds if the Perrot kinetic-energy functional (32b) is adopted.

Numerical solutions of the coupled equations (37)–(39) are easily obtained for any value of λ. Examples for a few values of λ are compared in Fig. 1 to the density profile $\rho_2(r)$ derived from the Perrot functional in the case of hydrogen ($Z = 1$). Only the value $\lambda = 1$ yields the exact cusp condition

TABLE I. Internal energy per ion (ϵ) and the pressure P/n_1 of the hydrogen plasma at $T=3\times10^3$ and 10^4 K, for $r_s=0.5$, 1, and 1.5. The various theories presented here are denoted as follows: (a) IS(0), the simple homogeneous electron gas model; (b) IS(P), the ion-sphere model of Sec. IV using the Perrot kinetic energy functional; (c) IS(W), same as (b) except that the von Weizsäcker functional is used ($\lambda=0.41$); (d) HNC, energy and pressure calculated from $g_{11}(r)$ and $g_{12}(r)$ of the present HNC-TFW theory (Sec. V) and Eqs. (60)–(62).

T (K)	r_s	ϵ (hartree)				P/n_1 (hartree)			
		IS(0)	IS(P)	IS(W)	HNC-TFW	IS(0)	IS(P)	IS(W)	HNC
10^4	0.5	1.703	1.629	1.646	1.910	2.041	2.013	2.048	2.224
3×10^3		1.703	1.629	1.646	1.773	2.041	2.013	2.048	2.132
10^4	1.0	-0.2532	-0.2969	-0.3283	-0.1755	0.2839	0.2854	0.2941	0.4216
3×10^3		-0.2532	-0.2969	-0.3283	-0.2534	0.2839	0.2854	0.2941	0.3558
10^4	1.5	-0.4144	-0.4571	-0.4993	-0.4446	0.0256	0.0357	0.0442	0.1334
3×10^3		-0.4144	-0.4571	-0.4993	-0.4959	0.0256	0.0357	0.0442	0.0817

$$\lim_{r\to0}\frac{d}{dr}\ln\rho_2(r)=-2, \qquad (40)$$

which is also satisfied by the Perrot functional. The latter, although presumably more accurate, is numerically much more demanding, particularly in the context of the HNC theory developed in Sec. V. For the sake of simplicity, it is natural to seek the ''optimum'' value of λ, which would lead to the best agreement between the results based on the kinetic-energy functionals (32a) and (32b). A possible criterion is to seek the value of λ that matches the ground-state energies:

$$E_0=E_K+E_C+E_X$$
$$=E_K-2\pi\int_0^{a_1}\rho_2(r)r\,dr-2\pi\int_0^{a_1}\rho_2(r)\Phi(r)r^2dr$$
$$+C_X4\pi\int_0^{a_1}[\rho_2(r)]^{4/3}r^2dr, \qquad (41)$$

where E_K is calculated from either Eq. (32a) or (32b) and E_C denotes the total Coulomb (potential) energy. This yields $\lambda\approx0.3$ at $r_s=0.5$ and $\lambda\approx0.70$ at $r_s=1$. Ground-state energies are listed in Table I, together with the corresponding values of the pressure, as deduced from the virial theorem

$$P=\frac{n_2}{3}[2E_K+E_C+E_X]. \qquad (42)$$

One can notice that the energy and pressure values predicted from either Eq. (32a) or (32b) are quite close. Note that the predictions of the ion-sphere model may be looked upon as representing approximately the zero-temperature limit of the ion-electron plasma, since each ion is assumed to be held fixed at the center of its sphere. It is interesting to compare our predictions to those of a simple IS model [9], where electron polarization is completely neglected, so that their contribution to the internal energy reduces to that of a uniform electron gas occupying the volume of the IS. The total energy and the virial pressure obtained from this model are shown in Table I. The difference between the ''rigid'' and

the ''responding'' electron-gas results is surprisingly small, as was already concluded from the linear screening results of Ref. [22].

V. ION-ION AND ION-ELECTRON CORRELATIONS

In order to determine the ion-ion and ion-electron pair distribution functions $g_{11}(r)$ and $g_{12}(r)$, we resort to Percus's identification of the latter with the spherically symmetric, normalized density profiles $\rho_1(r)/n_1$ and $\rho_2(r)/n_2$ of ions and electrons in the ''external field'' due to one ion assumed to be held fixed at the origin [4]. The dimensionless potentials $\Psi_\alpha(r)$ appearing in Eq. (16a) are correspondingly $\beta(\mu_1+Z^2/r)$ and $\beta(\mu_2-Z/r)$. Adopting the approximate ion-electron functional defined by Eqs. (27)–(31), with either Eq. (32a) or (32b) for the electron kinetic energy, the combination of the four equations (16a), (16b), (21a), and (21b) forms a closed set for the calculation of $g_{11}(r)$, $g_{12}(r)$, $c_{11}(r)$, and $c_{12}(r)$. The DCF $c_{22}(r)$ that enters the OZ relation (21b) is uniquely determined by the choice (31), with the LDA form (35) for E_X, namely, according to Eqs. (16b) and (18),

$$k_BTc_{22}(\mathbf{r}-\mathbf{r}')=-\frac{\delta^2\{E_H[\rho_2]+E_X[\rho_2]\}}{\delta\rho_2(\mathbf{r})\,\delta\rho_2(\mathbf{r}')}$$
$$=\frac{4}{9}C_X\frac{\delta(\mathbf{r}-\mathbf{r}')}{[\rho_2(\mathbf{r})]^{2/3}}-\frac{1}{|\mathbf{r}-\mathbf{r}'|}. \qquad (43)$$

Note that within the present approximation for the free-energy functional, the third OZ relation (21c) is not needed to close the system. Substituting Eqs. (27)–(29) into Eq. (16a) for $\alpha=1$, Percus's identification, together with the OZ relation (21a), leads directly to the HNC closure equation for $g_{11}(r)$:

$$g_{11}(r)=\exp\{-\beta v_{11}(r)+h_{11}(r)-c_{11}(r)\}, \qquad (44)$$

where $v_{11}(r)\equiv\phi_1(r)=Z^2/r$.

Similarly, substitution of Eqs. (28)–(30), (31), and (32a) into Eq. (16a) for $\alpha=2$ leads to the following integro-differential equation, which generalizes Eq. (37) to the present, multi-ion case:

$$\frac{\lambda}{8}\left\{\left[\frac{\rho_2{}'(r)}{\rho_2(r)}\right]^2 - \frac{2\rho_2{}''(r)}{\rho_2(r)} - \frac{4}{r}\frac{\rho_2{}'(r)}{\rho_2(r)}\right\} + \frac{5}{3}C_K[\rho_2(r)]^{2/3}$$

$$+ \frac{4}{3}C_X[\rho_2(r)]^{1/3} - \int\left[c_{12}(\mathbf{r}-\mathbf{r}') - \frac{1}{|\mathbf{r}-\mathbf{r}'|}\right]\rho_1(\mathbf{r}')d\mathbf{r}'$$

$$= \mu_2 - \Phi(r), \tag{45}$$

where the electrostatic potential

$$\Phi(r) = -v_{12}(r) + Z\int\frac{\rho_1(\mathbf{r}')}{|\mathbf{r}-\mathbf{r}'|}d\mathbf{r}' - \int\frac{\rho_2(\mathbf{r}')}{|\mathbf{r}-\mathbf{r}'|}d\mathbf{r}, \tag{46}$$

with $v_{12}(r) \equiv \phi_2(r) = -Z/r$, is a solution of Poisson's equation

$$\Phi''(r) + \frac{2}{r}\Phi'(r) = 4\pi[\rho_2(r) - Z\rho_1(r)] \tag{47}$$

satisfying the boundary conditions

$$\lim_{r\to 0} r\Phi(r) = Z, \tag{48a}$$

$$\Phi'(r=R) = 0. \tag{48b}$$

R is the radius of a sphere around the central ion, chosen sufficiently large for the density profiles to have reached their bulk values n_1 and n_2 within a given accuracy; in practice, R was chosen to be about $50a_1$ in the numerical calculations.

Equation (45), with $\rho_2 = n_2 g_{12}(r)$, provides the second closure relation. The associated OZ relations are given by Eqs. (22a) and (22b) in their $\mathbf{k}$-space representation. In the Appendix some details are given concerning the iterative solution of the closed set of equations (44), (45), (22a), and (22b).

A convenient but uncontrolled shortcut is provided by the mean-field approximation

$$k_BT c_{12}(r) \approx -v_{12}(r) = \frac{Z}{r}, \tag{49}$$

which greatly simplifies Eq. (45), since the latter now contains only the unknown functions $\rho_\alpha(r) = n_\alpha g_{1\alpha}(r)$ ($\alpha = 1,2$). With the ansatz (49), only three out of the four equations (44), (45), (22a), and (22b) are needed to close the system, but the latter is no longer self-consistent. For the sake of a comparison with the full (self-consistent) theory, we have solved the set of equations (44), (45), and (22a), assuming (49). The results from this set will be referred to as ''mean-field'' theory. They generally provide the input for an iterative solution of the full, self-consistent theory.

For the latter, we have systematically adopted the simpler, Thomas-Fermi plus square-gradient [TF-W(λ)] kinetic-energy functional (32a) rather than the more acurate Perrot functional (32b), which greatly complicates the numerical work. This leaves open the choice of the optimum value of the parameter λ in Eq. (32a). An energy criterion within the ion-sphere model was proposed in Sec. IV. Equating the ground-state energies derived from the two kinetic-energy functionals (32a) and (32b) leads to an optimum λ that varies

with r_s, but is independent of Γ (zero-temperature limit). An alternative criterion is based on the observation that linear-response theory yields an adequate description of electron screening at very high densities ($r_s < 1$), where the degenerate electrons are only weakly polarized by the external potential due to the ionic charge distribution [14]. The mean response of the Fourier component of the electron density to the latter is

$$\hat{\rho}_2(\mathbf{k}) \approx \langle\widetilde{\rho}_{2\mathbf{k}}\rangle_2 = \hat{\chi}_2(\mathbf{k})\widetilde{\rho}_{1\mathbf{k}}\hat{v}_{12}(k), \tag{50}$$

where $\hat{\rho}_2(\mathbf{k})$ is the FT of the electron density profile (9), which is obtained by averaging the FT of the electron density operator (3) over electronic degrees of freedom (symbolized by $\langle\ \rangle_2$) for a given ionic configuration characterized by the Fourier component $\widetilde{\rho}_{1\mathbf{k}}$ of the ionic density operator. For $r_s < 1$, local-field corrections are quite negligible, so the susceptibility $\hat{\chi}_2(\mathbf{k})$ is well approximated by the random-phase approximation [25]

$$\hat{\chi}_2(\mathbf{k}) = \frac{\hat{\chi}_2^{(0)}(\mathbf{k})}{1 - \hat{v}_{12}(k)\hat{\chi}_2^{(0)}(\mathbf{k})}, \tag{51}$$

where $\hat{\chi}_2^{(0)}(\mathbf{k})$ is the free-electron susceptibility, given by the Lindhard function (23). The resulting expression for the ion-electron PDF within the linear-response approximation reads [14]

$$n_2 g_{12}^{LR}(r) = \frac{1}{(2\pi)^3}\int d\mathbf{k}e^{i\mathbf{k}\cdot\mathbf{r}}\frac{1}{N}\langle\widetilde{\rho}_{1\mathbf{k}}\widetilde{\rho}_{2-\mathbf{k}}\rangle$$

$$\approx \frac{1}{(2\pi)^3}\int d\mathbf{k}e^{i\mathbf{k}\cdot\mathbf{r}}\hat{\chi}_2(\mathbf{k})S_{11}(k)\hat{v}_{12}(k). \tag{52}$$

$S_{11}(k)$ is taken to be the structure factor of the OCP (with electrons just providing a uniform background) in order to obtain $g_{12}(r)$ consistently to first order in the ion-electron coupling. λ is now adjusted so that the first minimum of $g_{12}^\lambda(r)$ coincides with that of $g_{12}^{LR}(r)$. We found that this procedure reproduces the overall structure of the electronic PDF better than a direct fitting by minimization of the mean-square deviation because of a slight dephasing of $g_{12}^\lambda(r)$ with respect to $g_{12}^{LR}(r)$ that appears at $r \geq a_1$ for $\lambda < 1$. The fitting to the linear-response result is justified at $r_s = 0.5$, where electrons are only weakly polarized by the ionic charge distribution. The optimization procedure yields $\lambda \approx 0.41$, nearly independently of Γ. This value will be kept throughout the subsequent calculations. A similar fitting carried out for $r_s = 1$, where linear response is much less justified [14], leads to an optimum value λ close to this adopted value of $\lambda = 0.41$. Explicit calculations of the pair structure were carried out for $r_s = 0.5$, 1, and 1.5 along two isotherms $T = 10^4$ and 3×10^3 K and along a constant coupling path ($\Gamma = 10$).

The relative inadequacy of the mean-field approximation embodied in Eq. (49), relative to the full self-consistent theory, is illustrated in Fig. 2, where the ion-ion structure factors are shown. The observed differences, particularly at small k (which governs the equation of state via the compressibility equation), are sufficiently large to warrant com-
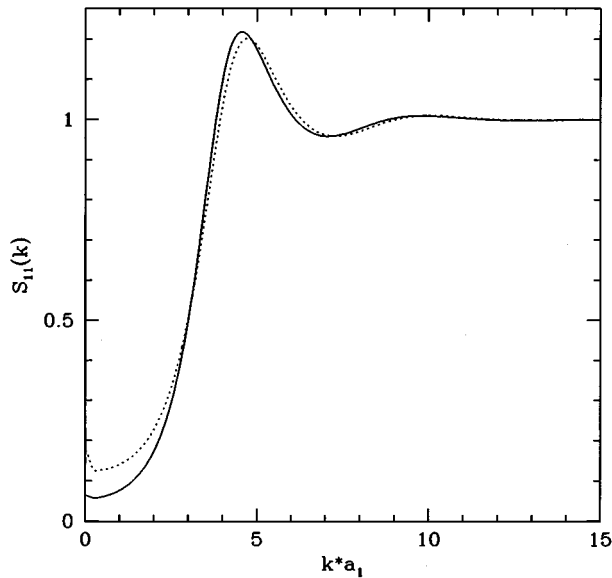
FIG. 2. $S_{11}(k)$ from the mean-field approximation (dotted line) compared to that obtained by the full self-consistent theory (solid line) with $\lambda = 0.41$.
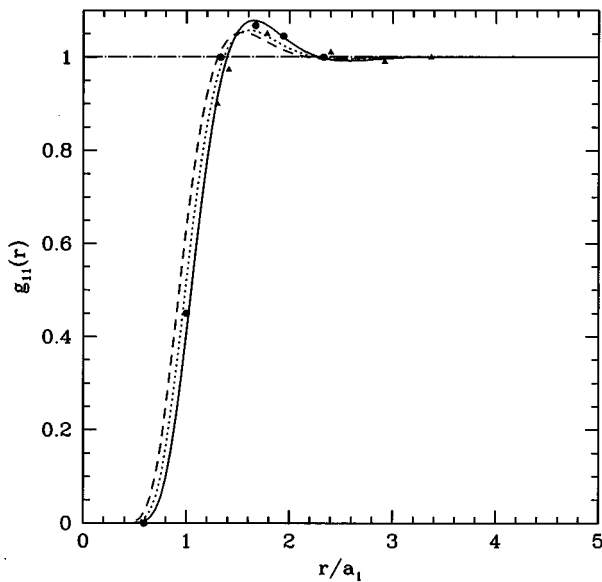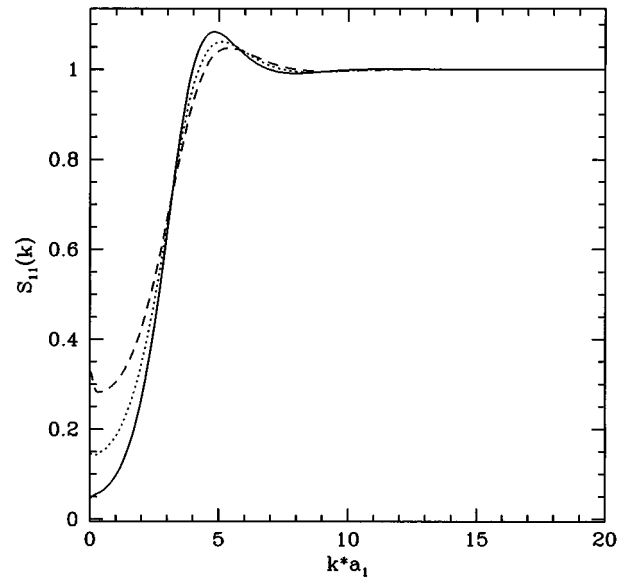

FIG. 4. $S_{11}(k)$ from the self-consistent HNC-TFW theory ($\lambda = 0.41$) versus ka_1 along the path $\Gamma = 10$ for $r_s = 0.5$ (solid line), 1 (dotted line), and 1.5 (dashed line).

plete self-consistent calculations throughout, despite the significantly larger numerical effort.

Results along the $\Gamma = 10$ path are shown in Figs. 3–5 and are compared with Chihara's quantum HNC (QHNC) results where available [7]. The qualitative tendencies are as expected, in particular the dramatic piling up of the electron density near the protons with increasing r_s, as shown by $g_{12}(r)$ in Fig. 5. Figure 4 exhibits strongly enhanced long-wavelength ion density fluctuations as r_s increases, which may be interpreted as precursors to atomic recombination, i.e., of a plasma phase transition [26]. Note, however, that the formation of H_2 molecules cannot be easily described

within the present theoretical framework.

Results along the $T = 10^4$ K isotherm are shown in Figs. 6–8. As expected, the ion-ion structure, represented by $g_{11}(r)$ in Fig. 6 and $S_{11}(k)$ in Fig. 7, diminishes dramatically as r_s increases, i.e., with increasing electron screening. The HNC results for $r_s = 0.5$ exhibit slightly less structure than the *ab initio* molecular-dynamics (MD) data [14], as might be expected from HNC theory. The enhancement of long-wavelength density fluctuations at $r_s = 1.5$ is again very significant, as seen from Fig. 7. The HNC results for $g_{12}(r)$ agree well with the *ab initio* MD data for ion-electron distances $r \gtrsim 0.5a$. The large differences at shorter distances result from a combination of two errors: The MD data, which
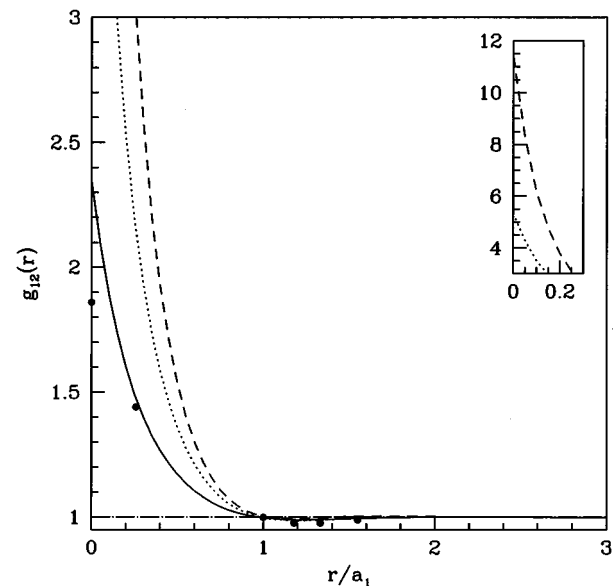

FIG. 3. $g_{11}(r)$ from the self-consistent HNC-TFW theory ($\lambda = 0.41$) versus r/a_1 along the path $\Gamma = 10$ for $r_s = 0.5$ (solid line), 1 (dotted line), and 1.5 (dashed line). The QHNC results of Chihara [7] are also shown at $r_s = 0.5$ ($\bullet$) and $r_s = 1$ ($\blacktriangle$).

FIG. 5. Same as Fig. 4, but representing $g_{12}(r)$ versus r/a_1. The QHNC results of Chihara [7] are also shown at $r_s = 0.5$ ($\bullet$).
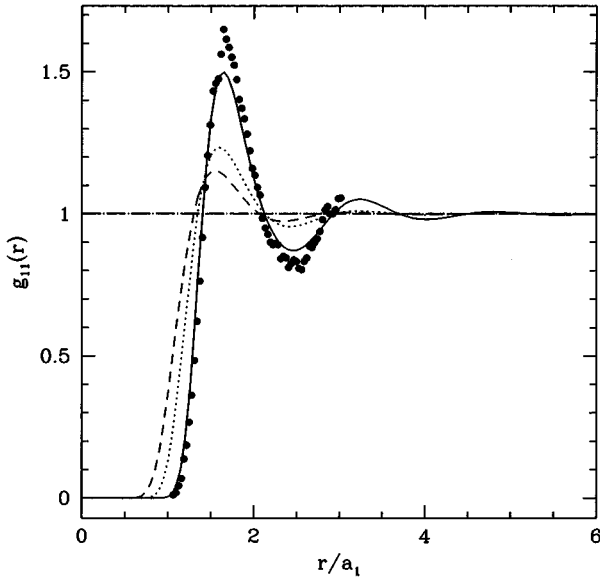
FIG. 6. $g_{11}(r)$ along the isotherm $T = 10\,000$ K for $r_s = 0.5$, 1, and 1.5. Curves for different r_s are denoted as in Fig. 4. Also shown are results from the MD simulation [14] for $r_s = 0.5$ (●).

are seen to have zero slope at the origin, are strongly affected by the energy cutoff in the plane-wave expansion of the Kohn-Sham orbitals, while the HNC results, although they correctly exhibit a nonzero slope, do not satisfy the exact cusp condition, which holds only if the choice $\lambda = 1$ is made in the square-gradient term.

Finally, Figs. 9–11 display the results for the lower-temperature isotherm $T = 3 \times 10^3$ K. The ion-ion pair structure for $r_s = 0.5$ and $r_s = 1$ [where $g_{11}(r)$ agrees well with the MD data, although the HNC results appear to be slightly more structured in this case] looks again as expected, but the results at $r_s = 1.5$ do not follow the pattern observed at higher temperature since they exhibit *more* structure than their $r_s = 1$ counterparts. There is once more a clear-cut enhance-
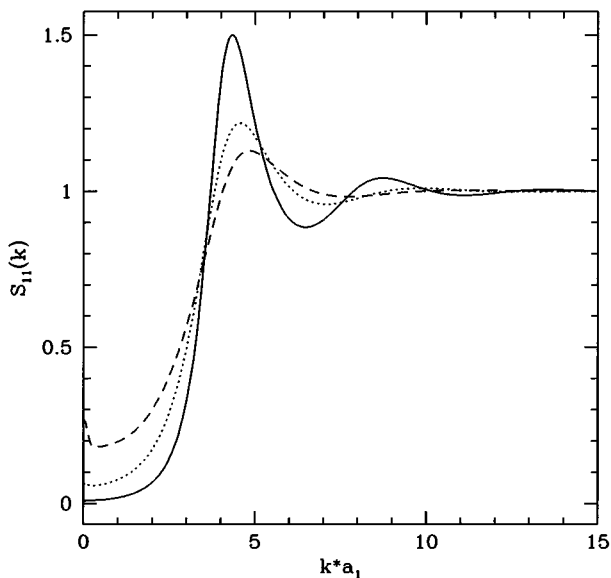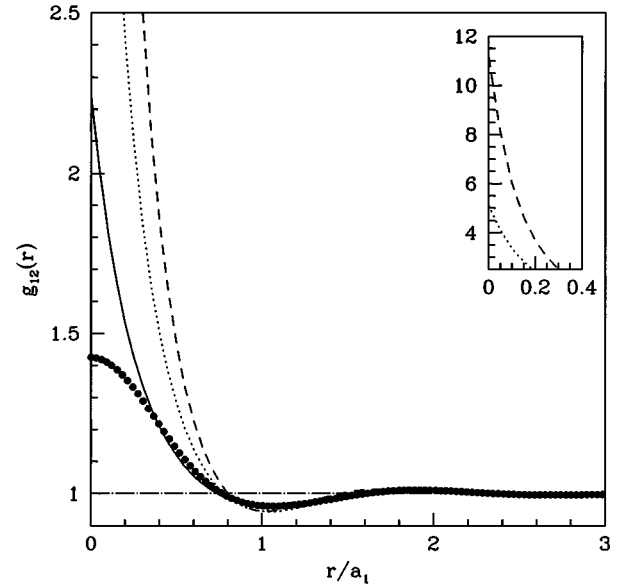

FIG. 8. Same as Fig. 6, but representing $g_{12}(r)$.

ment of $S_{11}(k)$ at small k. We are clearly in a situation where a naive electron screening picture is insufficient to explain the observed behavior, which may be, loosely speaking, associated with a plasma-insulator transition.

VI. REDUCTION TO AN EFFECTIVE ONE-COMPONENT SYSTEM

In asymmetric binary mixtures it is often instructive and convenient to reduce the initial two-component system to an effective one-component system involving only the properly ''dressed'' particles of the larger or heavier component by integrating out the degrees of freedom of the smaller (lighter) species. This is a customary procedure in the theory of metals, where averages are taken over the ground state of the
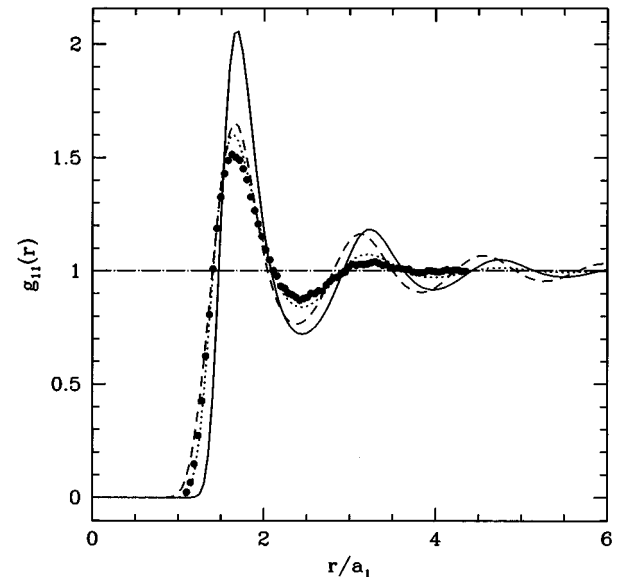

FIG. 7. Same as Fig. 4, but along the isotherm $T = 10\,000$ K.

FIG. 9. Same as Fig. 6, but along the isotherm $T = 3000$ K. The ● denote the MD simulation [14] results for $r_s = 1$.
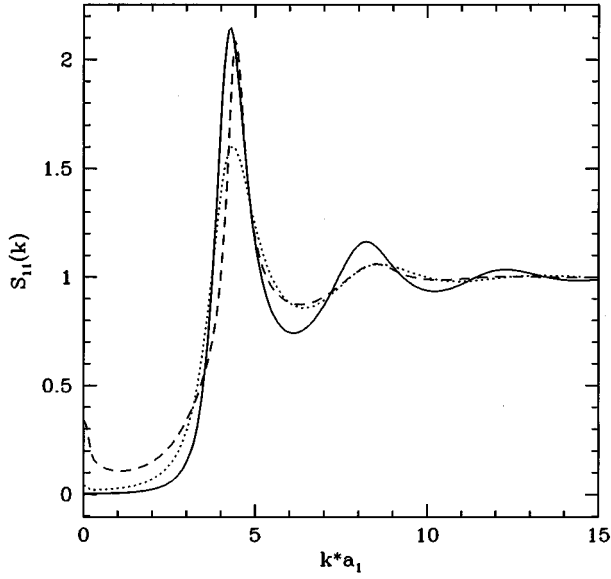
FIG. 10. Same as Fig. 4, but along the isotherm $T = 3000$ K.

conduction electrons, for any given configuration of the ions, leading to an effective, screened interaction between dressed ions or ''pseudoatoms'' [27]. A formal reduction of the initial ion-electron system to a one-component system of pseudoatoms can be carried out by a simple manipulation of the Ornstein-Zernike relations [28], and an expression for the effective pair potential between pseudoatoms can then be derived from the HNC closure [29]. The FT of the OZ relation (21a) reads

$$\hat{h}_{11}(k) = \hat{c}_{11}(k) + n_1 \hat{h}_{11}(k)\hat{c}_{11}(k) + n_2 \hat{h}_{12}(k)\hat{c}_{12}(k).$$
$$(53)$$

The corresponding OZ relation for the effective one-component system of pseudoatoms is

$$\hat{h}(k) = \hat{c}(k) + n\hat{h}(k)\hat{c}(k), \qquad (54)$$
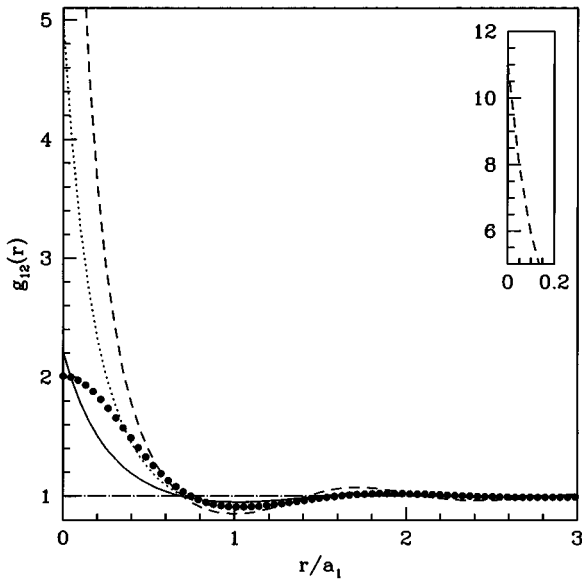

FIG. 11. Same as Fig. 9, but representing $g_{12}(r)$.

where $n = n_1$. By identifying $\hat{h}(k)$ with $\hat{h}_{11}(k)$ (the fluid of pseudoatoms is required to have a pair structure identical to that of the ions in the initial ion-electron plasma), one arrives immediately at the following expression for the DCF of the effective fluid in terms of the correlation functions of the ion-electron plasma:

$$\hat{c}(k) = \hat{c}_{11}(k) + \frac{n_2 \hat{h}_{12}(k)\hat{c}_{12}(k)}{S_{11}(k)}. \qquad (55)$$

To extract the effective pair potential between pseudoatoms, $v_{\text{eff}}(r)$, one compares the exact closure relations for $g_{11}(r)$ and $g(r)$, namely,

$$g_{11}(r) = \exp\{-\beta v_{11}(r) + h_{11}(r) - c_{11}(r) + B_{11}(r)\},$$
$$(56a)$$

$$g(r) = \exp\{-\beta v_{\text{eff}}(r) + h(r) - c(r) + B(r)\}, \quad (56b)$$

where $B(r)$ and $B_{11}(r)$ are the (unknown) bridge functions associated with the one and two-component representations of the plasma. Making once more the identification $g(r) \equiv g_{11}(r)$, and making the reasonable assumption that $B(r) = B_{11}(r)$ (the bridge functions are in fact taken to be identically zero in the HNC approximation), one arrives, with the help of Eq. (55), at the expression for the effective pair potential

$$\beta \hat{v}_{\text{eff}}(k) = \beta \hat{v}_{11}(k) - \frac{n_2 \hat{h}_{12}(k)\hat{c}_{12}(k)}{S_{11}(k)}. \qquad (57)$$

With the help of Eq. (21b), one easily checks that this expression for the FT of the effective potential is identical to that derived by Chihara [29]. It can be shown from the OZ relations (22b) and (22c) that if $\hat{h}_{12}(k)$ is approximated by its linear response limit (52), then $\hat{c}_{12}(k)$ reduces to the mean-field limit (49). Substituting these results into Eq. (57), the familiar temperature-independent expression for the effective ion-ion potential is recovered [19], namely,

$$\hat{v}_{\text{eff}}(k) = \hat{v}_{11}(k)[1 - \chi_2(k)\hat{v}_{12}(k)] = \frac{4\pi}{k^2} \frac{1}{\epsilon_2(k)}, \quad (58)$$

where $\epsilon_2(k)$ is the dielectric function of the homogeneous electron gas [25].

The HNC results for the pair structure of the ion-electron plasma, presented in Sec. V, have been used to compute the state-dependent effective pair potential. The variation of $v_{\text{eff}}(r)$ with r_s along the isotherms $T = 10^4$ and 3×10^3 K is shown in Figs. 12 and 13. As expected, the range of the effective interaction between dressed ions is seen to decrease dramatically as r_s increases. The importance of nonlinear screening as well as of temperature effects is illustrated by a comparison with the effective potential (58) valid in the linear screening regime, which is identical for the two temperatures. At the lowest density ($r_s = 1.5$), the nonlinear $v_{\text{eff}}(r)$ exhibits a shallow attractive well at the higher temperature and a marked oscillatory behavior at the lower temperature; the latter should not be confused with the familiar Friedel oscillations, which occur at larger distances and are a consequence of the singularity of the Lindhard function (23) at
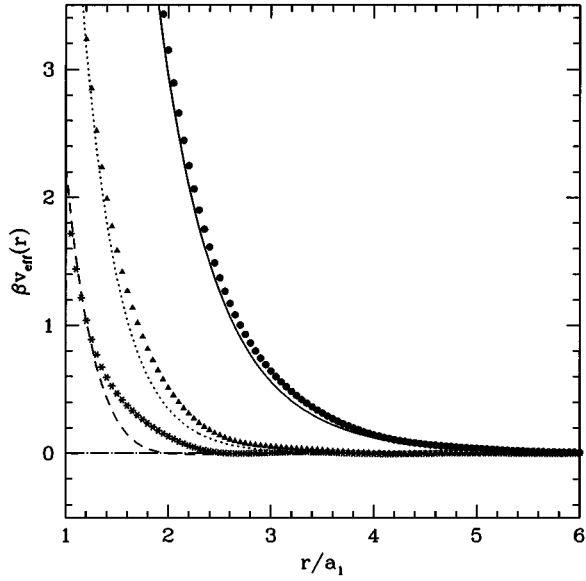
FIG. 12. Effective ion-ion pair potential $v_{\text{eff}}(r)$ reduced over $k_B T$ along the isotherm $T = 10\,000$ K for $r_s = 0.5$, 1, and 1.5. Curves for different r_s are denoted as in Fig. 4. Also shown are results from the linear-response theory [Eq. (58)], with ●, ▲, and * for $r_s = 0.5$, 1, and 1.5, respectively.

$k = 2k_F$ [25,27]. The oscillations seen in Fig. 13 rather reflect the strong ion-ion and ion-electron correlations at low temperatures and may be a signature of an incipient plasma-insulator transition [15].

VII. THERMODYNAMIC PROPERTIES

Explicit calculations of thermodynamic properties of ion-electron plasmas within the DFT framework have not been considered so far, except within the ion-sphere model [30]. This is due to the difficulty of deriving exact and operational expressions for the internal energy, the pressure, etc., from the pair distribution functions obtained in Sec. V. For purely
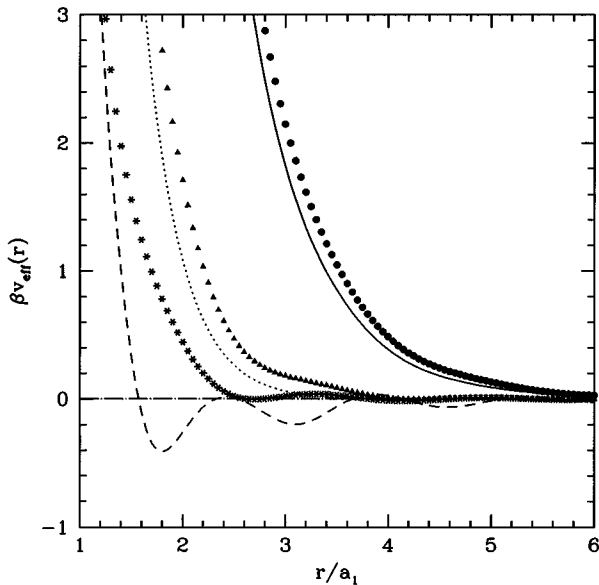

FIG. 13. Same as Fig. 12, but along the isotherm $T = 3000$ K.

classical systems, there exist three routes to thermodynamics, starting from the distribution functions, namely, the energy, virial, and compressibility routes [9]. The latter still holds for metallic systems composed of classical ions and degenerate electrons, as considered here; for a hydrogen plasma, the isothermal compressibility follows accordingly from [9]

$$\lim_{k \to 0} S_{11}(k) = \lim_{k \to 0} S_{12}(k) = \lim_{k \to 0} S_{22}(k) = n_1 k_B T \chi_T. \tag{59}$$

In practice, the structure factors calculated within the HNC–TF plus von Weizsäcker (TFW) scheme of Sec. V are extrapolated to $k = 0$ and the values of χ_T according to Eq. (59) are listed in Table II. The equation of state (pressure versus density along isotherms) requires a numerical integration of $\chi_T^{-1} = n(\partial P / \partial n)_T$. Turning to the energy route, it is clear that the (purely Coulombic) ion-ion and ion-electron contributions can be calculated from $g_{11}(r)$ and $g_{12}(r)$. The HNC-TFW theory does not yield $g_{22}(r)$, which would allow the electron-electron Coulomb energy to be evaluated, while the kinetic and exchange contributions cannot be expressed in terms of pair distribution functions alone. Approximate estimates of these contributions are obtained by substituting $\rho_2 = n_2 g_{12}(r)$ into the energy functional defined by Eqs. (31), (32a), (34) and (35), restricting the domain of integration to the volume of an ion sphere. The proposed expression for the internal energy per ion thus reads

$$\frac{E}{N_1} = \epsilon_K^1 + \epsilon_C^{11} + \epsilon_C^{12} + \epsilon_K^2 + \epsilon_C^{22} + \epsilon_X^2, \tag{60}$$

where

$$\epsilon_K^1 = \tfrac{3}{2} k_B T, \tag{61a}$$

$$\epsilon_C^{11} = 2 \pi n_1 \int_0^\infty v_{11}(r)[g_{11}(r) - 1] r^2 dr, \tag{61b}$$

$$\epsilon_C^{12} = 4 \pi n_2 \int_0^\infty v_{12}(r)[g_{12}(r) - 1] r^2 dr, \tag{61c}$$

$$\epsilon_K^2 = 4 \pi C_K n_2 \int_0^{a_1} [g_{12}(r)]^{5/3} r^2 dr$$
$$+ \frac{\pi \lambda}{2} n_2 \int_0^{a_1} \frac{[g'_{12}(r)]^2}{g_{12}(r)} r^2 dr, \tag{61d}$$

$$\epsilon_C^{22} = \frac{n_2^2}{2} \int_{r < a_1} d\mathbf{r} \int_{r' < a_1} d\mathbf{r}' v_{22}(|\mathbf{r} - \mathbf{r}'|)[g_{12}(r) - 1]$$
$$\times [g_{12}(r') - 1], \tag{61e}$$

$$\epsilon_X^2 = 4 \pi C_X n_2 \int_0^{a_1} [g_{12}(r)]^{4/3} r^2 dr. \tag{61f}$$

The same approximation leads, via the virial route, to the expression for the equation of state

$$\frac{P}{n_1 k_B T} = 1 + \frac{1}{3 k_B T} [\epsilon_C^{11} + \epsilon_C^{12} + 2 \epsilon_K^2 + \epsilon_C^{22} + \epsilon_X^2]. \tag{62}$$

TABLE II. Isothermal compressibility (χ_T) of the hydrogen plasma at $T = 3 \times 10^3$ and 10^4 K, for $r_s = 0.5$, 1, and 1.5. Columns 4–6 are obtained by a numerical differentiation of the virial equations (42) and (62), while the values of columns 3–5 are based on ion-sphere models (cf. Table I for notations) and those of columns 6 [denoted HNC(v)] are based on our HNC-TFW theory [cf. Eqs. (60)–(62)]. The last column [HNC(c)] represents χ_T given by the fluctuation relation (59).

		χ_T (a_B^3/hartree)				
T (K)	r_s	IS(0)	IS(P)	IS(W)	HNC(v)	HNC(c)
10^4	0.5	0.1416	0.1423	0.1402	0.1353	0.1489
3×10^3		0.1416	0.1423	0.1402	0.1470	0.1495
10^4	1.0	6.725	6.712	6.646	5.539	8.418
3×10^3		6.725	6.712	6.646	6.109	17.83
10^4	1.5	99.04	101.2	98.30	60.54	121.5
3×10^3		99.04	101.2	98.30	75.62	506.3

Estimates of the thermodynamic properties based on these approximate expressions are listed in Table I and compared with the predictions of the simple ion-sphere model introduced in Sec. IV. Compressibilities obtained by numerical differentiation of the virial pressure (62) are compared in Table II with the compressibilities calculated from the exact fluctuation relation (59). The agreement is satisfactory for $r_s = 0.5$ and $r_s = 1$ at the higher temperature ($T = 10^4$ K), but deteriorates for $r_s = 1$ at the lower temperature ($T = 3 \times 10^3$ K) and generally for $r_s = 1.5$, where χ_T increases rapidly. This large discrepancy may be ascribed to the approximate nature of the virial expression (62) for the pressure and to the familiar thermodynamic inconsistency of the HNC closure [9].

VIII. CONCLUSIONS

The present paper introduces a simple DFT of ion-electron plasmas, which avoids using the Kohn-Sham orbitals and yet compares favorably with earlier formulations based on the latter. The good accuracy of the theory, evaluated relative to the scarcely available *ab initio* MD simulations, is due to the introduction of gradient corrections to the TF theory, provided the crucial prefactor λ is determined by a confrontation with the predictions of linear-response theory of very high densities ($r_s = 0.5$). The theory is easily implemented numerically. An attempt has been made to derive the equation of state of the ion-electron plasma from these correlation functions; the calculated energies and pressures are surprisingly close to the predictions of the much simpler ion-sphere model, which ignores ion-ion correlations and hence cannot provide $g_{11}(r)$.

The pair structure calculated at the lowest density considered in this work ($r_s = 1.5$) exhibits a marked qualitative difference between the high- ($T = 10^4$ K) and low-temperature ($T = 3 \times 10^3$ K) results. Although the present theory cannot, of course, account for genuine bound states, the low-T data may be interpreted in terms of an incipient plasma-insulator transition, where the insulator phase contains recombined ion-electron pairs, i.e., atoms. The ''symptoms'' of such a recombination are the enhanced ion-ion structure observed at $r_s = 1.5$, relative to that obtained at higher densities, the significant enhancement of long-wavelength ion density fluctuations, as evidenced by $S_{11}(k)$

in the $k \to 0$ limit, and the marked oscillatory behavior of the effective ion-ion pair potential shown in Fig. 13. A further indication is the rapidly increasing difficulty of achieving convergence of the HNC-TFW equations as r_s increases beyond 1.5. Such a lack of convergence is usually associated with the proximity of a phase transition.

Despite many efforts in that direction, the plasma-insulator transtion in hydrogen is far from being understood. Because in its present form the DFT theory put forth in this paper cannot properly account for the molecular phase, the observed low-density behavior can only be looked upon as indicative. To obtain a clear picture of the scenario of the plasma-insulator transition, we plan to consider the simpler situation of spin-polarized hydrogen, which excludes the formation of H_2 molecules from the outset; this case will require only minor modifications of the present theory. We also plan to extend the DFT theory to H-He mixtures under very high pressures, for which a demixing transition has been predicted [31,32] and for which *ab initio* MD data recently have become available [33].

APPENDIX

We give here some details concerning the numerical solution of the self-consistent theory for the pair correlations displayed in Sec. V. The closed set of equations containing the unknown pair functions $h_{11}(r)$, $h_{12}(r)$, $c_{11}(r)$, $c_{12}(r)$, and $c_{22}(r)$ are given by Eqs. (22a), (22b), and (43)–(45), complemented by the definition of the potential $\Phi(r)$ in Eq. (46) and the Poisson equation (47) obeyed by $\Phi(r)$. We notice also that Eq. (43) gives directly $c_{22}(r)$ in the LDA approximation.

To start the iteration loop, an initial guess of $c_{12}(r)$, $h_{12}(r)$, and $\gamma(r) \equiv h_{11}(r) - c_{11}(r)$ is made. A convenient initial guess for $c_{12}(r)$ is its mean-field approximation $c_{12}(r) = -\beta v_{12}(r)$. The following steps are then taken at the $(n+1)$th iteration.

(a) The HNC integral equation (44) is solved by following

the numerical method proposed by Ng [34], except that we use here the Anderson mixing scheme [35]. The R space is discretized with segments of size $\delta r = 0.05 a_1$. Convergence is achieved if the norm of the difference of $\gamma(r)$ (as defined by Ng) between two consecutive iterations is less than 10^{-10}. This step yields $h_{11}^{(n+1)}(r)$ and $c_{11}^{(n+1)}(r)$.

(b) With $g_{11}(r) = h_{11}(r) + 1$ obtained in (a), we solve the coupled second-order ordinary differential equations (45) and (46) for $g_{12}(r)$ and the auxiliary function $\Phi(r)$. The boundary conditions for the potential function $\Phi(r)$ are given by Eqs. (48a) and (48b); those for $g_{12}(r)$ are simply $\lim_{r \to 0} r^2 g_{12}(r) = 0$ and $g_{12}(r = R) = 1$, where R is the radius of the larger sphere surrounding the central ion ($R \approx 50 a_1$), representing the boundary of our system. The numerical method used is a ''relaxation method'' [36] consisting of first replacing the ordinary differential equations by approximate finite-difference equations and then solving the latter using a multidimensional Newton's method by taking into account the boundary conditions. The initial guess ''relaxes''

then to the solution of the finite-difference equations. We have divided the system length R into segments of size $h = R/2048 = 0.025 a_1$ in order to have a good resolution of Eqs. (45) and (46). The tolerance parameter (controlling the convergence) is set to 10^{-14}. This step gives us $g_{12}^{(n+1)}(r)$ in the iteration process.

(c) The Fourier transforms of $h_{11}^{(n+1)}(r)$ and $h_{12}^{(n+1)}(r)$ obtained by (a) and (b) are injected into the right-hand side of a slightly rearranged form of the OZ relation (22b), i.e.,

$$\hat{c}_{12}(k) = \frac{n_2 \hat{h}_{12}(k)}{S_{11}(k)} \left[\frac{1}{\chi_2^{(0)}(k)} - \hat{c}_{22}(k) \right].$$

The self-consistency of the solutions is achieved if the right-hand side [representing $c_{12}^{(n+1)}(r)$] and the input from the preceding iteration, $c_{12}^{(n)}(r)$, agree within 0.01%. Otherwise, a mixing of $c_{12}^{(n+1)}$ and $c_{12}^{(n)}$ is processed and the iteration loop returns to point (a).

[1] P. Hohenberg and W. Kohn, Phys. Rev. **136**, B864 (1964).

[2] W. Kohn and L. J. Sham, Phys. Rev. **140**, A1133 (1965).

[3] N. D. Mermin, Phys. Rev. **137**, A1441 (1965).

[4] J. K. Percus, Phys. Rev. Lett. **8**, 462 (1962).

[5] H. Xu, J. P. Hansen, and D. Chandler, Europhys. Lett. **26**, 419 (1994).

[6] M. W. C. Dharma-wardana and F. Perrot, Phys. Rev. A **26**, 2096 (1982).

[7] J. Chihara, Phys. Rev. A **33**, 2575 (1986), and references therein.

[8] D. Ofer, E. Nardi, and Y. Rosenfeld, Phys. Rev. A **38**, 5801 (1988).

[9] See, e.g., J. P. Hansen and I. R. McDonald, *Theory of Simple Liquids*, 2nd ed. (Academic, London, 1986).

[10] R. Car and M. Parrinello, Phys. Rev. Lett. **55**, 2471 (1985).

[11] J. Clérouin, G. Zérah, D. Benisti, and J. P. Hansen, Europhys. Lett. **13**, 685 (1990); G. Zérah, J. Clérouin, and E. L. Pollock, Phys. Rev. Lett. **69**, 446 (1992); J. Clérouin, E. L. Pollock, and G. Zérah, Phys. Rev. A **46**, 5130 (1992).

[12] M. Pearson, E. Smargiassi, and P. A. Madden, J. Phys.: Condens. Matter **5**, 3221 (1993).

[13] E. Smargiassi and P. A. Madden, Phys. Rev. B **49**, 5220 (1994).

[14] J. Kohanoff and J. P. Hansen, Phys. Rev. E **54**, 768 (1996).

[15] The high-density molecular phase of hydrogen has been explored by D. Hohl, V. Natoli, D. M. Ceperley, and R. M. Martin, Phys. Rev. Lett. **71**, 541 (1993).

[16] See, e.g., R. G. Parr and W. Yang, *Density Functional Theory*

of Atoms and Molecules (Oxford University Press, New York, 1989).

[17] F. Perrot, J. Phys.: Condens. Matter **6**, 431 (1994).

[18] J. Chihara, J. Phys.: Condens. Matter **3**, 8715 (1991).

[19] N. W. Ashcroft and D. Stroud, Solid State Phys. **33**, 1 (1978).

[20] See, e.g., M. Baus and J. P. Hansen, Phys. Rep. **59**, 1 (1980); S. Ichimaru, H. Iyetomi, and S. Tanaka, *ibid.* **149**, 91 (1987).

[21] E. P. Wigner, Phys. Rev. **46**, 1002 (1934).

[22] S. Galam and J. P. Hansen, Phys. Rev. **148**, A816 (1976).

[23] R. Kubo, Rep. Prog. Phys. **19**, 255 (1966).

[24] J. Lindhard, K. Dan. Vidensk. Selsk. Mat. Fys. Medd. **28**, No. 8 (1954).

[25] D. Pines and Ph. Nozières, *The Theory of Quantum Liquids* (Benjamin, New York, 1976).

[26] D. Saumon and G. Chabrier, Phys. Rev. A **46**, 2084 (1992).

[27] T. Faber, *An Introduction to the Theory of Liquid Metals* (Cambridge University Press, Cambridge, 1972).

[28] S. A. Adelman, J. Chem. Phys. **64**, 724 (1976).

[29] J. Chihara, J. Phys. C **19**, 1665 (1986).

[30] See, e.g., F. Perrot, Phys. Rev. A **20**, 586 (1979).

[31] D. J. Stevenson, Phys. Rev. B **12**, 3999 (1975).

[32] J. P. Hansen, G. M. Torrie, and P. Viellefosse, Phys. Rev. A **16**, 2153 (1977).

[33] O. Pfaffenzeller, D. Hohl, and P. Ballone, Phys. Rev. Lett. **74**, 2599 (1995).

[34] K. C. Ng, J. Chem. Phys. **61**, 2680 (1974).

[35] D. R. Hamann, Phys. Rev. Lett. **42**, 662 (1979).

[36] *Numerical Recipes*, edited by W. H. Press *et al.* (Cambridge University Press, Cambridge, 1989).